

pubs.acs.org/cm Article

Lithiation in 2H-MoTe₂ Nanoflakes

Published as part of Chemistry of Materials special issue "In Memory of Prof. Francis DiSalvo". Shiyu Xu, Natalie L. Williams, Sihun Lee, Jason J. Huang, Saif Siddique, Andrej Singer, and Judy J. Cha*



Cite This: https://doi.org/10.1021/acs.chemmater.4c01517



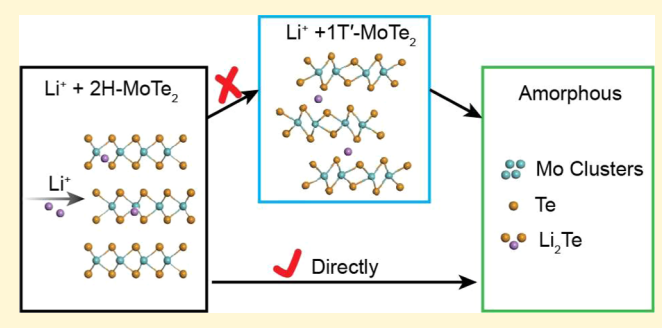
ACCESS

III Metrics & More

Article Recommendations

s Supporting Information

ABSTRACT: In several two-dimensional (2D) transition metal dichalcogenides (TMDs), lithium intercalation has been observed to induce a phase transition from the 2H phase to the 1T' phase in the TMDs, leading to improvements in various applications. For MoTe₂, calculations have also predicted the same phase transition under the influence of electron doping, strain, or lithium intercalation. In this work, however, we experimentally demonstrate that electrochemically controlled lithium intercalation does not lead to the predicted phase change in 2H-MoTe₂. Instead, the 2H-MoTe₂ directly decomposes to molybdenum (Mo), tellurium (Te), and lithium telluride (Li₂Te) upon lithiation despite the significant



electron doping achieved by the lithium intercalation into 2H-MoTe₂ flakes, probed using *in situ* Raman spectroscopy and *in situ* conductivity measurements. Performing the lithium intercalation on 2H-MoTe₂ flakes at higher temperatures also did not result in the 1T' phase, suggesting that additional thermal energy did not facilitate the phase transition. Thus, our experiments directly challenge the theoretical prediction and point to a potentially high nucleation barrier for the 1T' phase in MoTe₂. Our findings emphasize the importance of studying the phase transition pathways for lithium intercalation-induced phase transitions in 2D TMDs.

INTRODUCTION

The manipulation of phases in two-dimensional (2D) group VI transition metal dichalcogenides (TMDs) has been extensively researched due to their potential applications in cutting-edge fields such as optoelectronics, electronics, catalysis, and energy storage.¹⁻⁴ Molybdenum ditelluride (MoTe₂), a group VI TMD, has three primary polytypes with distinct electronic properties: semiconducting α - or 2H-MoTe₂, semimetallic β or 1T'-MoTe₂ that is also a higher order topological insulator,⁵ and γ- or T_d-MoTe₂ that is a ferroelectric Weyl semimetal.⁶ Calculations show that the energy difference between the ground state 2H phase and the metastable 1T' phase is merely 0.04 eV per formula unit, and a phase transition between the two phases should easily be achievable with both phases stable at room temperature.8 Various methods, including defect engineering,⁹ charge doping,^{10,11} strain engineering,^{7,12} intercalation, 13,14 thermal treatment, 8,15,16 and light irradiation, 17,18 can induce the phase transition between the two phases in MoTe₂. Yet, such transitions have been observed predominantly in the monolayer limit or only the surface layers of bulk crystals. For instance, Eshete et al. observed the 2H to 1T' transition only in the top and bottom layers of 2H-MoTe $_2$ nanoflakes immersed in an n-butyllithium solution at 110 $^{\circ}$ C. 14 Wang et al. demonstrated a reversible phase change between the 2H and 1T' phases using ionic liquid gating in monolayer

MoTe₂. ¹⁰ Zakhidov et al. replicated the findings on a 73-nm thick MoTe₂ nanoflake, observing that the newly formed 1T' phase is restricted to the surface layer. ¹¹ These experimental reports call into question whether a complete and reversible phase transition from the 2H phase to the 1T' phase is possible for MoTe₂ despite the theoretical predictions.

Here, we investigate the electrochemical intercalation of lithium (Li) into 2H-MoTe₂ nanoflakes to probe the theoretically predicted 2H to 1T' phase change in MoTe₂. We use lithium intercalation as previous research has demonstrated the phase transition from the 2H to 1T (or 1T') phase in MoS₂ and MoSe₂ through electrochemical Li intercalation, ^{19–23} which introduces significant amounts of electron doping and strain to the host system to induce the phase transition. ^{7,12,24} Our experiments show that intercalated Li⁺ indeed introduces electron doping to 2H-MoTe₂, as evidenced by the downshift and broadening of the A_{1g} peak in the Raman spectra during intercalation and the increased

Received: May 29, 2024 Revised: September 21, 2024 Accepted: September 23, 2024



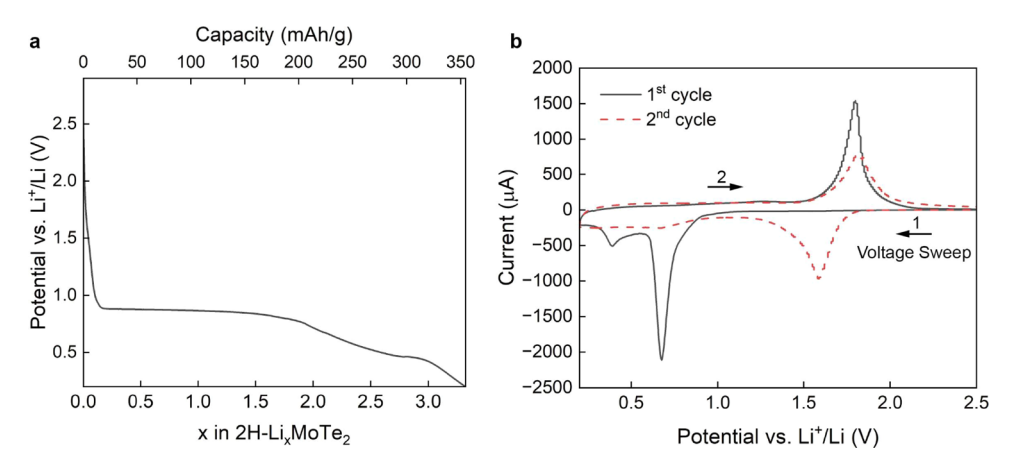


Figure 1. Electrochemical characteristics of 2H-MoTe₂. (a) Galvanostatic discharging of 2H-MoTe₂ powder in a coin cell at a current of 0.104 mA in the voltage window of 2.5 to 0.2 V vs Li⁺/Li. (b) Cyclic voltammogram traces of 2H-MoTe₂ vs Li⁺/Li in a coin cell at a scan rate of 4 mV/min.

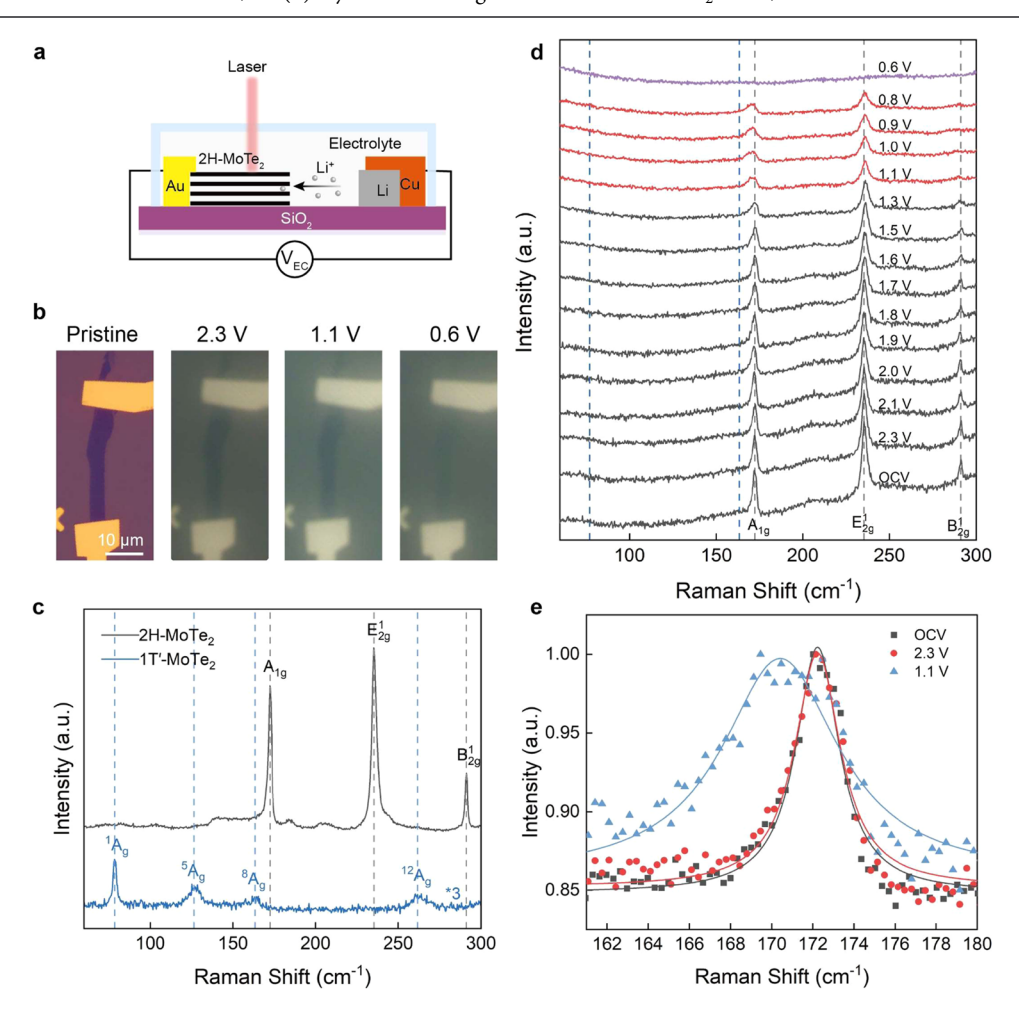


Figure 2. Lithium intercalation of a bilayer 2H-MoTe₂ nanoflake. (a) Schematic of a planar electrochemical intercalation cell with capabilities of *in situ* Raman and *in situ* two-terminal electrical measurements. V_{EC} stands for the electrochemical intercalation voltage applied between the single crystalline 2H-MoTe₂ nanoflake and the Li⁺/Li electrode. (b) Optical images of a bilayer 2H-MoTe₂ nanoflake as a function of V_{EC} ; scale bar, 10 μ m. (c) Raman spectra of bilayer 2H-MoTe₂ (black) and 1T'-MoTe₂ (blue, thickness ~10 nm) nanoflakes. (d) *In situ* Raman spectra of the 2H-MoTe₂ nanoflake in (b) as a function of V_{EC} . The black and red spectra represent the Raman-active peaks without and with obvious shifts and broadening, respectively. The topmost purple spectrum represents the amorphous state. The blue vertical dashed lines indicate the characteristic peak positions of 1T'-MoTe₂. (e) Raman spectra at V_{EC} = OCV (in black), 2.3 V (in red), and 1.1 V (in blue) ν s Li⁺/Li, along with their corresponding Lorentz fitting curves.

conductivity of the flake with Li intercalation. Yet, in situ Raman spectroscopy indicates that 2H-MoTe₂ does not transition to the 1T' phase through electrochemical Li

intercalation; instead, 2H-MoTe $_2$ decomposes directly to molybdenum (Mo), tellurium (Te), and lithium telluride (Li_2 Te) at an applied electrochemical voltage (V_{EC}) of 0.6–0.8

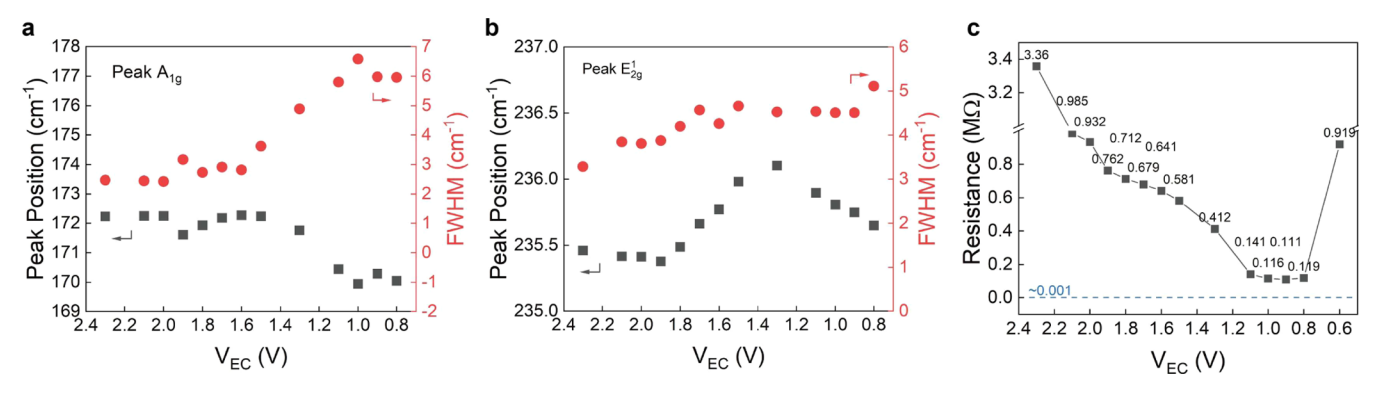


Figure 3. Peak position and full width at half-maximum (FWHM) of the (a) A_{1g} and (b) E_{2g}^1 mode of bilayer 2H-MoTe₂ at different applied V_{EC} . (c) Measured resistance of the bilayer 2H-MoTe₂ nanoflake at different applied V_{EC} . The blue dashed line indicates a typical resistance value of a bilayer 1T'-MoTe₂ nanoflake. Figure S1 shows the full I-V characteristics.

V vs Li⁺/Li using liquid electrolyte (1 M LiPF₆ in a 50:50 v/v EC/DEC solution), with flake thicknesses ranging from bilayer to ~90 nm. Increasing the temperature during lithium intercalation up to 100 °C did not induce the phase transition while the intercalation kinetics were accelerated. This study thus shows that, despite the theoretical calculations that suggest the Li-intercalated 1T′-MoTe₂ should be more thermodynamically stable than the 2H phase, the phase transition is not experimentally realized in MoTe₂ nanoflakes. Our findings suggest a potentially high nucleation barrier between the two phases for MoTe₂ and highlight the importance of studying phase transition pathways in TMDs.

RESULTS AND DISCUSSION

Electrochemical Characteristics of 2H-MoTe₂ Powder.

Coin-type electrochemical cells were constructed to characterize the lithiation process of 2H-MoTe₂ powder (with sizes smaller than 38 μ m, details in Experimental Methods section). Only one single reduction peak was observed during lithiation as proven by both the galvanostatic discharge curve showing a voltage plateau at 0.8 V vs Li⁺/Li in Figure 1a and by the cyclic voltammetry trace with a reduction peak at 0.7 V vs Li⁺/Li in the black trace in Figure 1b. This reduction peak during the first lithiation cycle signifies the irreversible decomposition reaction from 2H-MoTe₂ to an amorphous state containing a mixture of Mo, Te, and Li_2Te , consistent with previous findings reported in 1987. The oxidation peak observed at 1.8 V vs Li⁺/Li in the first cycle (Figure 1b, black trace) and the two reduction-oxidation (redox) peaks observed at 1.6 and 1.8 V vs Li⁺/Li in the second cycle (Figure 1b, red dashed trace) correspond to the lithiation and delithiation of pure Te.²

Electrochemical Intercalation in Bilayer 2H-MoTe₂ Nanoflakes. Since recent studies suggest the 2H to 1T' phase transition in MoTe₂ is limited to the surface layers or monolayers, 10,11,14 it is possible that the lithiation using MoTe₂ powder, where the particle sizes are in the μ m range, will not show the signature of the 1T' phase. We thus explore the lithium intercalation into thin 2H-MoTe₂ flakes employing electrochemical intercalation cells, which enable real-time *in situ* Raman spectroscopy and two-terminal electrical measurements during Li intercalation at various applied electrochemical voltages (V_{EC}) (Figure 2a, Experimental Methods section). By applying a V_{EC} between the single-crystalline 2H-MoTe₂ nanoflake (cathode) and Li (anode), lithium ions (Li⁺) are inserted into the van der Waals (vdW) gaps of the 2H-

 $MoTe_2$ nanoflake. The applied V_{EC} ranges between the open-circuit voltage (OCV, typically 2.3–2.8 V $\textit{vs}\ Li^+/Li)$ and 0.1 V $\textit{vs}\ Li^+/Li$. A lower V_{EC} corresponds to a higher Li concentration in the $2H\text{-}MoTe_2$ nanoflake.

Figure 2b shows optical images of a bilayer 2H-MoTe₂ nanoflake under various V_{EC} values (the left most image labeled "Pristine" is before applying the electrolyte to the flake, while the rest of the images are taken with the flake submerged under the electrolyte). Figure 2c presents Raman spectra of the pristine 2H-MoTe₂ nanoflake with characteristic Raman modes of A_{1g} , E_{2g}^1 , and B_{2g}^1 and of a pristine 1T'-MoTe₂ nanoflake with characteristic Raman modes of ¹Ag, ⁵Ag, ⁸Ag, and ¹²Ag in accordance with the references. ^{27,28} We determine the 2H-MoTe₂ nanoflake to be a bilayer owing to the lack of the Davydov splitting of the A_{1g} mode,²⁹ the small A_{1g}/E^{1}_{2g} peak intensity ratio,³⁰ and the presence of the B_{2g}^1 mode at 291.2 cm⁻¹, which is absent in monolayer MoTe₂.³¹ As the V_{EC} was swept from OCV to 0.8 V vs Li⁺/Li, Raman spectra were taken at a 0.1 V decrement (Figure 2d). Lithium intercalation induced electron doping in 2H-MoTe2, which is evident in the shift and broadening of active peaks in the Raman spectra. Figure 2e shows the A_{1g} Raman peak in detail at $V_{EC} = OCV$, 2.3 V, and 1.1 V vs Li⁺/Li.³² The A_{lg} mode shifts to lower wavenumbers and broadens considerably. Eventually, amorphization of 2H-MoTe $_2$ occurs when the V_{EC} drops below 0.6 V vs Li⁺/Li, as denoted by the purple featureless Raman spectrum in Figure 2d (topmost spectrum). We note that throughout the entire intercalation process, no Raman peaks that match the 1T' phase of MoTe₂ were observed.

Figure 3 shows further analysis of the changing Raman modes with lithium intercalation. From V_{EC} = OCV to 0.8 V νs Li+/Li, the peak position and full width at half-maximum (FWHM) of the A_{lg} mode was tracked, showing the response of MoTe₂ to lithium intercalation (Figure 3a). Concurrently, the E¹_{2g} peak shifts upward by 0.6 cm⁻¹, starting from 235.4 ${\rm cm}^{-1}$ at ${\rm V_{EC}} = {\rm OCV}$ to 236.1 ${\rm cm}^{-1}$ at ${\rm V_{EC}} = 1.5~{\rm V}$ vs ${\rm Li}^+/{\rm Li}$, and then shifts back to 235.6 cm⁻¹ at $V_{EC} = 0.8 \text{ V } \text{ vs Li}^+/\text{Li}$. The FWHM of the E¹_{2g} peak also increases from 3.3 to 5.1 cm⁻¹ from $V_{EC} = OCV$ to 0.8 V vs Li⁺/Li, as shown in Figure 3b. Additionally, the B_{2g}^1 peak disappears when the V_{EC} < 1.1 V vs Li⁺/Li (Figure 2d). These findings indicate the successful intercalation of Li⁺ into the 2H-MoTe₂ nanoflake, which leads to electron doping in the system.³² The A_{1g} mode exhibits greater sensitivity to this n-type doping compared to the E12g mode. While gradually decreasing in intensity, the A_{1g} and E_{2g}^{1} peaks of the 2H-MoTe₂ persist throughout the intercalation

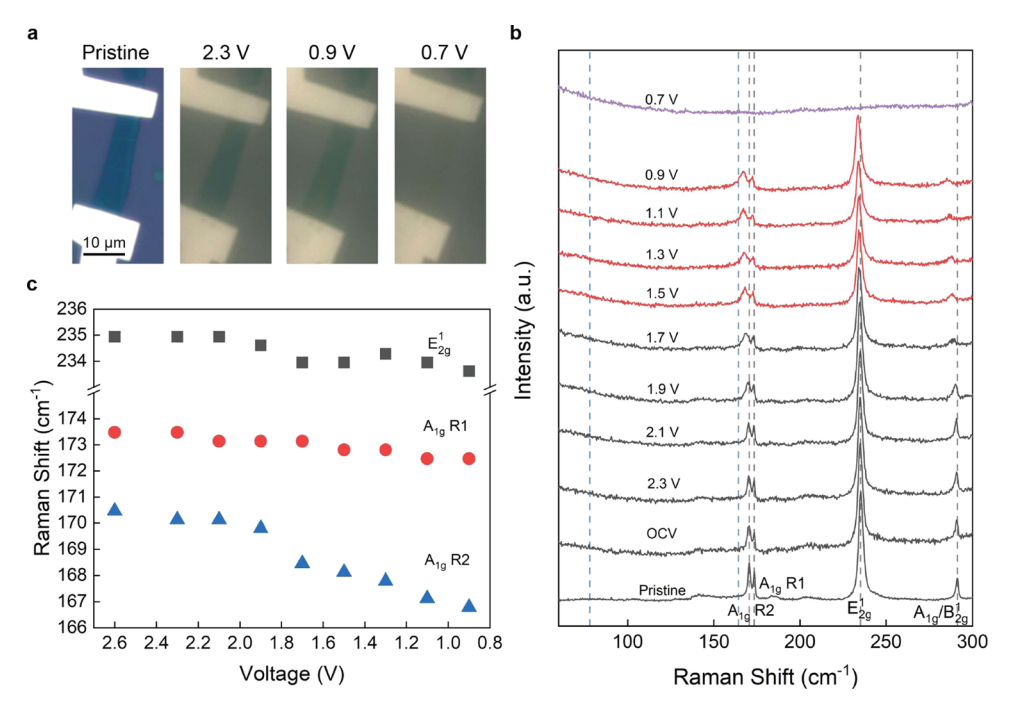


Figure 4. Lithium intercalation of a 4-layered 2H-MoTe₂ nanoflake. (a) Optical images as a function of V_{EC} using a liquid electrolyte; scale bar, 10 μ m. (b) In situ Raman spectra of the 2H-MoTe₂ nanoflake in (a) as a function of V_{EC} . The black ($V_{EC} = OCV - 1.7 \text{ V vs Li}^+/Li$) and red ($V_{EC} = 1.5 - 0.9 \text{ V vs Li}^+/Li$) spectra represent the Raman-active peaks without and with obvious shifts and broadening, respectively. The purple topmost spectrum ($V_{EC} = 0.7 \text{ V vs Li}^+/Li$) represents the amorphous state. (c) Peak positions of E^1_{2g} , A_{1g} R1 and A_{1g} R2 Raman modes of 4-layered 2H-MoTe₂ at different applied V_{EC} .

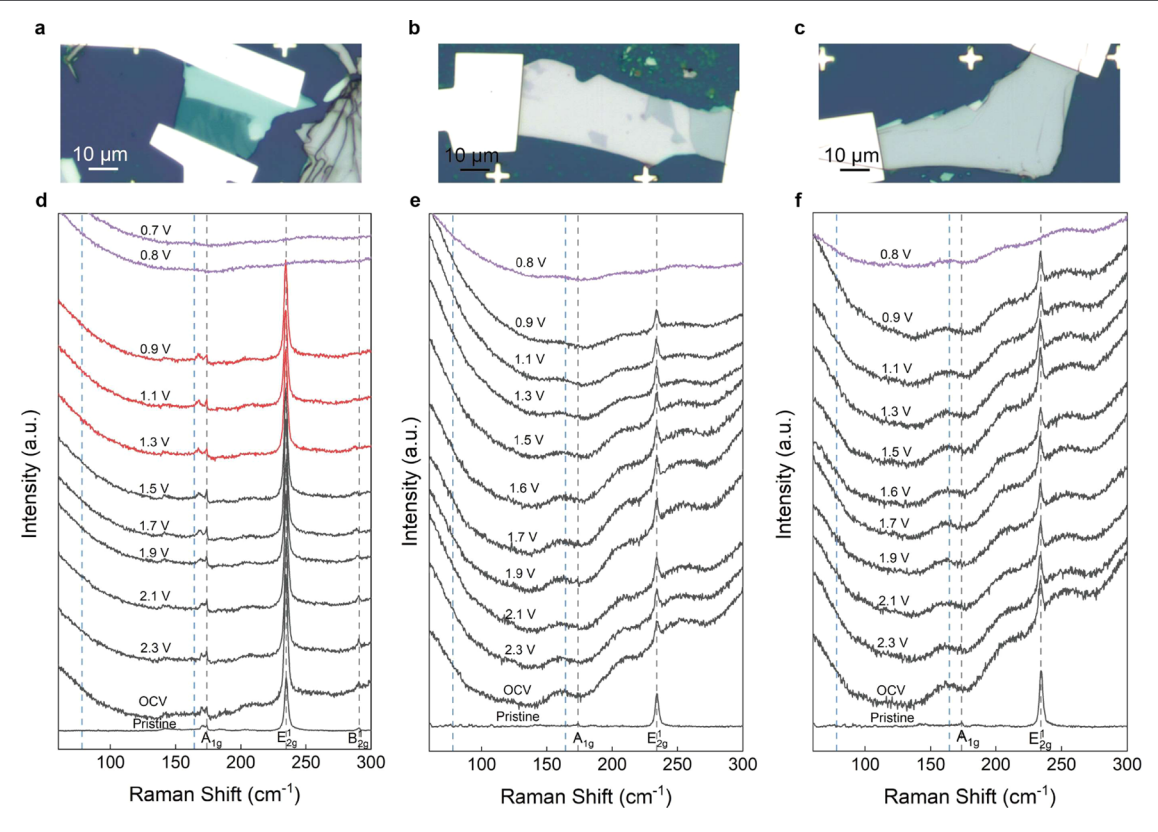


Figure 5. Lithium intercalation of thick 2H-MoTe₂ nanoflakes with various thicknesses. Optical images of pristine 2H-MoTe₂ nanoflakes of (a) 5 or 6 layers, (b) \sim 40 nm and (c) \sim 90 nm; scale bar, 10 μ m. (d-f) In situ Raman spectra of the 2H-MoTe₂ nanoflakes in (a-c) as a function of V_{EC} using a liquid electrolyte, respectively. The black and red spectra represent the Raman-active peaks without and with obvious shifts and broadening, respectively. The purple spectra represent the amorphous states.

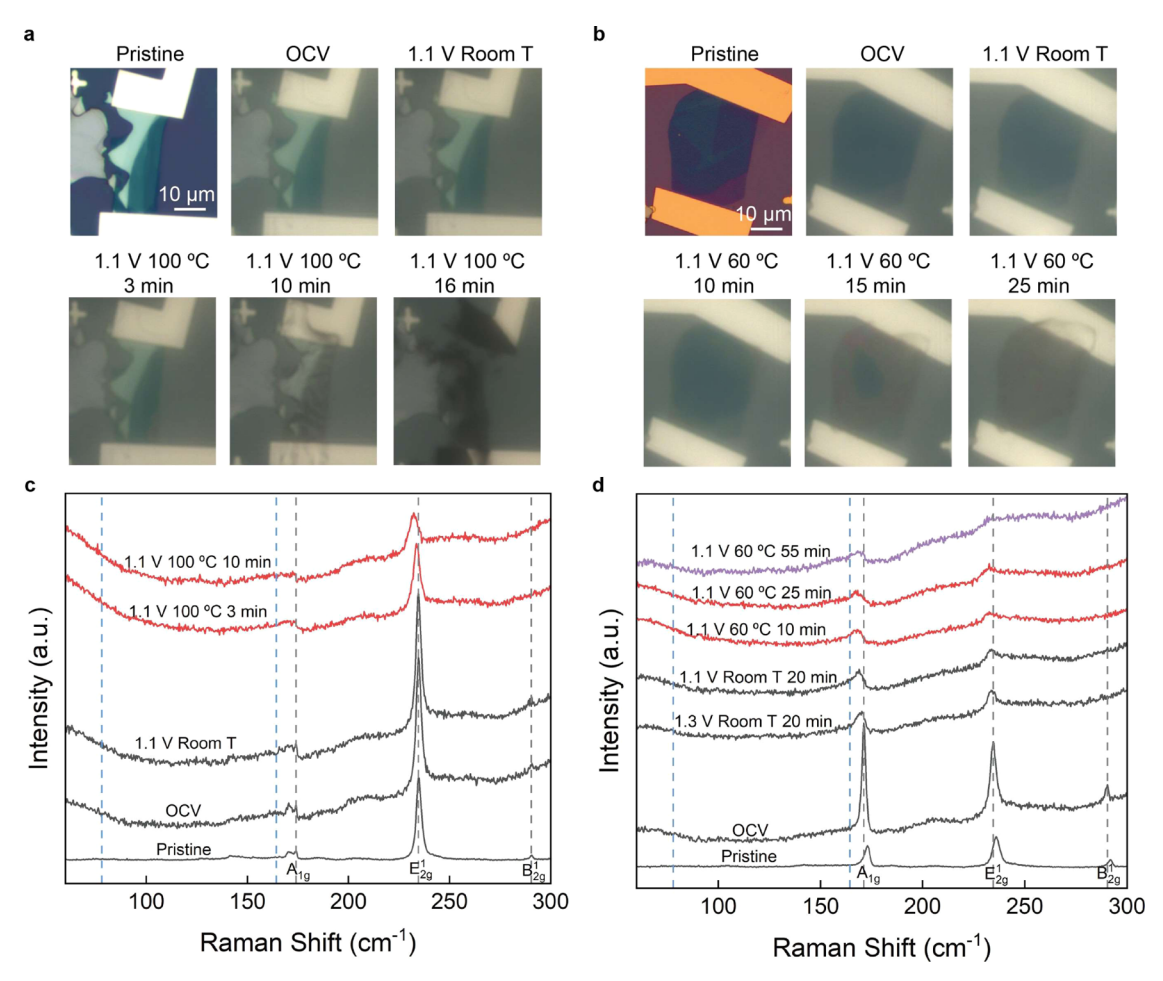


Figure 6. Lithium intercalation of liquid cells on 2H-MoTe $_2$ nanoflakes at high temperatures. Optical images of pristine few-layered 2H-MoTe $_2$ nanoflakes for intercalation experiments conducted at (a) 100 °C and (b) 60 °C, respectively; scale bar, $10 \, \mu m$. (c, d) In situ Raman spectra of the few-layered 2H-MoTe $_2$ nanoflakes in (a) and (b), respectively, as a function of V_{EC} , time and temperature. The black and red spectra represent the Raman-active peaks without and with obvious shifts and broadening, respectively. The purple spectrum represents the amorphous state.

process. No Raman modes of the $1\mathrm{T'}$ -MoTe₂ at \sim 78 or \sim 164 cm⁻¹ (the blue dashed lines in Figure 2d) are observed during intercalation. Therefore, we conclude that bilayer 2H-MoTe₂ does not transition to the $1\mathrm{T'}$ phase via electrochemical lithium intercalation but instead directly decomposes into Mo, Te, and Li₂Te at $V_{EC}=0.6~\mathrm{V}~vs~\mathrm{Li^+/Li.^{25}}$

The electrical and transport characteristics of the same bilayer 2H-MoTe₂ nanoflake were assessed across varying V_{EC} (Figure 3c). The two-terminal resistance of the 2H-MoTe₂ nanoflake decreased from ${\sim}1$ to ${\sim}0.1~M\Omega$ as the V_{EC} decreased, indicating an increased conductivity due to the electron doping by the intercalation of Li⁺. Nevertheless, even in the deeply lithiated state, the resistance of the flake was at least 2 orders of magnitude higher than typical resistance values of metallic 1T'-MoTe2 flakes with similar dimensions (See Figure S1 for the I-V curves of the bilayer 2H-MoTe₂ flake during lithiation and 1T'-MoTe2 devices), which suggests that lithium intercalation did not induce the 1T' phase, consistent with the Raman data (Figure 2d). The resistance of the bilayer 2H-MoTe $_2$ flake rose to ~ 1 M Ω following amorphization at $V_{EC} = 0.6 \text{ V } vs \text{ Li}^+/\text{Li}$. The observed change in resistance during lithiation reinforces our finding that 2H-MoTe₂ does not transition to the 1T' phase through lithium intercalation but rather directly decomposes.

Electrochemical Intercalation in 2H-MoTe₂ Nano-flakes with Different Thicknesses. The absence of the 2H to 1T' phase transition in bilayer MoTe₂ nanoflakes during lithiation might be due to its thickness. Theoretical calculations suggest that thinner 2H-MoS₂ flakes face increased difficulty transitioning to the 1T' phase, as the flake thickness influences both the energy difference between the two phases and the critical electron concentration required for the phase transition.^{33,34} Experiments indicate that reducing the thickness of MoS₂ below five layers hinders the kinetics of the 2H to 1T' phase transition induced by lithium intercalation.²³ This is attributed to heightened interfacial effects between MoS₂ nanoflakes and the SiO₂/Si substrate, suppressing the growth rate of the 1T' domain. Therefore, it is plausible that the 2H-1T' phase transition in MoTe₂ is influenced by its thickness.

To test this hypothesis, we performed lithium intercalation on thicker 2H-MoTe $_2$ flakes (4 layers, 5–6 layers, ~40, and 90 nm in thickness). Figure 4a show optical images of a 4-layered 2H-MoTe $_2$ nanoflake under various V_{EC} values, and its thickness was confirmed through Davydov splitting of the A_{1g} mode into two peaks using a 633 nm laser and optical contrast on a 300 nm SiO $_2$ /Si substrate. A the V_{EC} is reduced from OCV to 0.9 V vs Li $^+$ /Li, Raman peaks of A_{1g} R1, A_{1g} R2, and E_{2g}^1 undergo downshifts (Figure 4b,c) to indicate successful intercalation. Amorphization occurs at $V_{EC}=0.7$ V

vs Li⁺/Li. No Raman peaks corresponding to the 1T' phase are observed. Figure 5 shows optical images and Raman spectra of 2H-MoTe₂ nanoflakes of 5-6 layers, ~40, and ~90 nm thicknesses based on the optical contrast on the 300 nm SiO₂/ Si substrate. Even though the intensity of the $A_{\rm lg}$ peak is low in flakes thicker than \sim 40 nm, the primary E_{2g}^1 peak persists, and no Raman peaks belonging to the 1T' phase appear during the lithiation process before the flakes transition to an amorphous state, which confirms the absence of a phase transition from 2H to 1T'. The amorphization voltage increases from V_{EC} = 0.6 to 0.8 V vs Li⁺/Li when the flake is thicker than 6 layers. Figure S2 shows the optical images and in situ Raman spectra of a ${\sim}20$ nm thick $2H\text{-MoTe}_2$ nanoflake as a function of V_{EC} during Li intercalation, and the selected area electron diffraction (SAED) pattern of the nanoflake post-Li intercalation. The nanoflake became amorphous at 1.0 V, confirmed by SAED of the Li-intercalated nanoflake showing the characteristic rings of an amorphous material.

Electrochemical Intercalation of 2H-MoTe₂ Nanoflakes at High Temperatures. It is plausible that the lack of phase transition may have to do with a high nucleation barrier or very slow growth rate for the T' phase. From calculations, the phase transition from 2H-MoTe₂ to 1T'-MoTe₂ may require a high energy barrier (E_b) of more than 0.8 eV per $MoTe_2$ formula unit as well as the large Te displacement of more than 1 Å. According to the classical nucleation theory, the nucleation rate R follows the Arrhenius equation: $R = Ae^{-\frac{\Delta G^{*}}{k_B T}}$, where A is an intrinsic coefficient associated with the material, ΔG^* is the free energy of the nucleus, $k_{\rm B}$ is the Boltzmann constant, and T is the temperature. 35 Increasing the temperature has the potential to accelerate the nucleation and growth rate of the 1T'-MoTe₂. Since 2H-MoTe₂ can convert to the 1T' phase at 500 °C anneal by inducing Te vacancies, we performed lithium intercalation while heating the sample at 60 and 100 °C, well below 500 °C.8 Degradation of the liquid electrolyte prevented us from heating above 100 °C.

Figure 6a displays optical images of a few-layered 2H-MoTe₂ nanoflake at a V_{EC} = 1.1 V νs Li⁺/Li and a temperature of 100 °C. The flake exhibited rapid wrinkling at 10 min, turned dark, and became disconnected from the Cr/Au electrodes at 16 min. As shown in the Raman spectra in Figure 6c, the A_{1g} and E_{2g} peaks remained stable at room temperature; however, upon heating the cell to 100 °C, the A_{1g} peak disappeared quickly, and the E¹_{2g} peak experienced a significant downshift. Still, Raman peaks associated with the 1T' phase did not emerge. Another heating experiment was conducted at 60 °C, allowing us more time to observe the intercalation process. Figure 6b shows optical images of a few-layered 2H-MoTe₂ flake during lithiation, heated to 60 °C at a $V_{EC} = 1.1 \text{ V} \text{ vs Li}^+/$ Li. From 10 to 25 min, the 2H-MoTe₂ flake darkened, starting from the edge, indicating the occurrence of the amorphization reaction. Raman spectra confirmed a rapid downshift and broadening of both the A_{1g} and E_{2g}^1 peaks at 60 °C and at V_{EC} = 1.1 V vs Li⁺/Li (Figure 6d). Amorphization occurred at the same $V_{EC} = 1.1 \text{ V vs Li}^+/\text{Li}$ at 55 min, a considerably higher applied voltage than the amorphization voltage of 2H-MoTe₂ flakes at room temperature ($V_{EC} = 0.8 \text{ V vs Li}^+/\text{Li}$). In situ Raman inspection during lithium intercalation indicated that no 1T' phase emerged at 100 or 60 °C. Therefore, heating only accelerated the intercalation process and amorphization

but did not induce the phase transition from 2H to $1T^\prime$ phases in MoTe₂ nanoflakes.

CONCLUSIONS

In summary, our study reveals that, despite theoretical predictions that suggest thermodynamic stability of lithiumintercalated 1T'-MoTe2 over the 2H phase, this stability was not observed experimentally for nanoflakes with thicknesses between bilayer and 90 nm. This discrepancy may be attributed to a substantial nucleation barrier for the 1T' phase, preventing its realization under the applied electrochemical voltage at room temperature. Notably, conducting experiments up to 100 °C did not yield any observable phase transitions before the amorphization. Since many theoretical calculations are based on bulk or monolayer TMDs, crucial factors such as interlayer interactions and strain involved during intercalation and phase change are overlooked. Consequently, our findings underscore the significance of considering phase transition pathways, along with the final phases at thermodynamic equilibrium, in understanding intercalation-induced phase transitions in 2D TMDs.

■ EXPERIMENTAL METHODS

Assembly of Coin-Type Cells. 2H-MoTe₂ bulk crystals (HQ Graphene) were ground using an agate mortar and pestle and sieved to sizes smaller than 38 μ m through a 400-mesh USA standard sieve. The finely sieved crystals were mixed with 5 wt % acetylene black and 5 wt % poly(vinylidene fluoride) (PVDF) in NMP, resulting in the formation of a slurry. The slurry was uniformly cast onto a doubleside-carbon-coated aluminum foil (MSE Supplies) using a doctor blade and dried at 50 °C in an Ar glovebox overnight, forming the cathode sheet with an active loading of approximately 4 mg/cm². To minimize edge defects, the cathode sheet was sandwiched between two weighing papers before being cut into cathode electrode disks with a diameter of 15 mm, using a disc punching tool. The subsequent assembly of CR 2032 cells was sealed with a crimping machine, incorporating lithium disks with a 15.6 mm diameter as the anode, 20 mm-diameter Celgard 3501 separators, battery-grade 1 M lithium hexafluorophosphate (LiPF₆ in a 50:50 v/v EC/DEC solution, Sigma-Aldrich) as the electrolyte, and the cathode electrode disks serving as the cathode. Prior to experiments, the cells were kept at least 24 hours within the argon-filled glovebox.

Device Fabrication. Multilayer flakes of $2H\text{-MoTe}_2$ were obtained through mechanical exfoliation from bulk crystals of $2H\text{-MoTe}_2$ (2D Semiconductors) using the scotch-tape method. The flakes were then transferred onto a SiO_2/Si substrate using a potassium hydroxide (KOH)-assisted transfer method with poly-(propylene carbonate) (PPC, Sigma-Aldrich). The multilayer exfoliated $2H\text{-MoTe}_2$ flakes were placed on a 300 nm SiO_2/Si substrate with alignment marks designed for electron-beam lithography. Subsequently, electrodes were defined through scanning electron microscope (SEM)-based electron beam lithography (Quanta 200F SEM with NPGS Lithography), followed by the deposition of 10 nm chromium (Cr) and 100 nm gold (Au) through thermal evaporation using Mbraun EcoVap.

Fabrication of Electrochemical Intercalation Cells. All electrochemical intercalation cells followed a consistent planar cell configuration, featuring a 2H-MoTe₂ nanoflake as the working electrode and a small Li metal piece (approximately 3 mm by 3 mm, 0.38 mm-thick ribbon, Sigma-Aldrich) as the counter/reference electrode. The constructed 2H-MoTe₂ device was enclosed with a Li electrode within a transparent case, including an optical-grade glass top cover. This case was then filled with a liquid electrolyte (1 M lithium hexafluorophosphate in 50:50 v/v ethylene carbonate/diethyl carbonate, LiPF₆ in EC/DEC, Sigma-Aldrich). All procedures for assembling the electrochemical intercalation cells were executed

within an argon glovebox, ensuring O_2 and H_2O levels were maintained below 0.5 ppm.

In Situ Raman Characterization. Lithium intercalation was carried out using a Biologic SP300 potentiostat, which applied an electrochemical voltage (V_{EC}) between the Cr/Au electrode of the $2H\text{-}MoTe_2$ flake (functioning as the working electrode) and the Li electrode (serving as the reference/counter electrode). Raman spectroscopy, known for its sensitivity and noninvasiveness, was used to detect structural changes in the 2H-phased flake during lithium intercalation. In situ Raman spectra were recorded using a HORIBA LabRAM HR Evolution Spectrometer using a 633 nm He-Ne laser featuring an 1800 lines/mm diffraction grating. To prevent laser-induced damage to the flake, a laser power was kept at \sim 3 mW. Before intercalation, a Raman spectrum was obtained at the open circuit voltage (OCV), typically within the range of 2.3 to 2.8 V vs Li⁺/Li for 2H-MoTe₂ intercalation cells. Throughout the electrochemical intercalation process, V_{EC} was gradually reduced at a controlled rate of 10 mV/s, and then maintained at desired voltages while multiple Raman spectra were collected. Concurrently, optical images were captured using the Raman microscope's camera. Differences in contrast and brightness observed between the pristine 2H-MoTe₂ and other optical images during intercalation were attributed to the presence of the electrolyte and coverslip.

In Situ Two-Terminal Electrical Measurements. Two-terminal electrical measurements were carried out in situ using a semi-conductor device analyzer (Agilent Technologies B1500A) while lithium intercalation was ongoing. A drain—source voltage of 50 mV was applied, and the resistance was determined using Ohm's law, extracted from the slope of the I-V curve through a linear regression method.

Scanning Transmission Electron Microscopy (STEM) Characterization. For selected area electron diffraction (SAED), intercalated 2H-MoTe $_2$ flakes were washed with isopropyl alcohol and transferred onto SiN_x TEM grids using KOH-assisted polymer stamping method. The TEM grids were then cleaned with Ar/O_2 plasma. The SAED patterns were collected on a Thermo Fisher Scientific Spectra 300 X-CFEG at an accelerating voltage of 300 kV.

ASSOCIATED CONTENT

Supporting Information

The Supporting Information is available free of charge at https://pubs.acs.org/doi/10.1021/acs.chemmater.4c01517.

Two-terminal resistance measurements of $2H\text{-MoTe}_2$ during intercalation and $1T'\text{-MoTe}_2$ (S1), $2H\text{-MoTe}_2$ intercalation Raman spectra and post intercalation STEM-HAADF and SAED characterization (S2) (PDF)

AUTHOR INFORMATION

Corresponding Author

Judy J. Cha – Department of Materials Science and Engineering, Cornell University, Ithaca, New York 14853, United States; orcid.org/0000-0002-6346-2814; Email: jc476@cornell.edu

Authors

Shiyu Xu — Department of Materials Science and Engineering, Cornell University, Ithaca, New York 14853, United States; Department of Mechanical Engineering and Materials Science, Yale University, New Haven, Connecticut 06511, United States; orcid.org/0000-0002-3061-632X

Natalie L. Williams – Department of Materials Science and Engineering, Cornell University, Ithaca, New York 14853, United States; Department of Chemistry and Chemical Biology, Cornell University, Ithaca, New York 14853, United States; Oorcid.org/0009-0007-8526-3481

Sihun Lee – Department of Materials Science and Engineering, Cornell University, Ithaca, New York 14853, United States

Jason J. Huang — Department of Materials Science and Engineering, Cornell University, Ithaca, New York 14853, United States; orcid.org/0000-0002-6387-1650

Saif Siddique — Department of Materials Science and Engineering, Cornell University, Ithaca, New York 14853, United States

Andrej Singer — Department of Materials Science and Engineering, Cornell University, Ithaca, New York 14853, United States; © orcid.org/0000-0002-2965-9242

Complete contact information is available at: https://pubs.acs.org/10.1021/acs.chemmater.4c01517

Author Contributions

"S.X. and N.L.W. contributed equally to this work. S.X. and J.J.C. conceived the project. S.X., N.L.W. and S.L. carried out the experiments and analyzed the data. J.J.H. and A.S. assembled and tested the coin-type cells. S. S. performed STEM characterization. S.X. and J.J.C. wrote the manuscript with input from all authors. All authors have given approval to the final version of the manuscript.

Notes

The authors declare no competing financial interest.

ACKNOWLEDGMENTS

S.X. and J.J.C. gratefully acknowledge support from the National Science Foundation (NSF CBET #2240944). Device fabrication and characterization were partly carried out at the Yale West Campus Materials Characterization Core and the Yale West Campus Cleanroom. This work was also performed in part at the Cornell NanoScale Facility, a member of the National Nanotechnology Coordinated Infrastructure (NNCI), which is supported by NSF (Grant NNCI-2025233). The authors acknowledge the use of facilities and instrumentation supported by NSF through the Cornell University Materials Research Science and Engineering Center DMR- 1719875, and the Platform for the Accelerated Realization, Analysis, and Discovery of Interface Materials (PARADIM) Award No. DMR-2039380.

■ REFERENCES

- (1) Kim, J. H.; Sung, H.; Lee, G.-H. Phase Engineering of Two-Dimensional Transition Metal Dichalcogenides. *Small Sci.* **2024**, 4 (1), No. 2300093.
- (2) Nikitina, A. A.; Lavrentev, F. V.; Yurova, V. Y.; Piarnits, D. Y.; Volkova, O. O.; Skorb, E. V.; Shchukin, D. G. Layered nanomaterials for renewable energy generation and storage. *Mater. Adv.* **2024**, 5 (2), 304–408
- (3) Li, X.; Aftab, S.; Hussain, S.; Kabir, F.; Al-Sehemi, A. G.; Aslam, M.; Kim, J. H.; Goud, B. S. Progress in photodetector devices utilizing transition metal dichalcogenides. *J. Mater. Chem. C* **2024**, *12* (4), 1211–1232.
- (4) Wang, M.; Xu, S.; Cha, J. J. Revisiting Intercalation-Induced Phase Transitions in 2D Group VI Transition Metal Dichalcogenides. *Adv. Energy Sustainable Res.* **2021**, 2 (8), No. 2100027.
- (5) Wang, Z.; Wieder, B. J.; Li, J.; Yan, B.; Bernevig, B. A. Higher-Order Topology, Monopole Nodal Lines, and the Origin of Large Fermi Arcs in Transition Metal Dichalcogenides XTe₂ (X = Mo, W). *Phys. Rev. Lett.* **2019**, *123* (18), No. 186401.
- (6) Wang, Z.; Gresch, D.; Soluyanov, A. A.; Xie, W.; Kushwaha, S.; Dai, X.; Troyer, M.; Cava, R. J.; Bernevig, B. A. MoTe₂: A Type-II Weyl Topological Metal. *Phys. Rev. Lett.* **2016**, *117* (5), No. 056805.

- (7) Duerloo, K.-A. N.; Li, Y.; Reed, E. J. Structural phase transitions in two-dimensional Mo- and W-dichalcogenide monolayers. *Nat. Commun.* **2014**, *5* (1), No. 4214.
- (8) Keum, D. H.; Cho, S.; Kim, J. H.; Choe, D.-H.; Sung, H.-J.; Kan, M.; Kang, H.; Hwang, J.-Y.; Kim, S. W.; Yang, H.; Chang, K. J.; Lee, Y. H. Bandgap opening in few-layered monoclinic MoTe₂. *Nat. Phys.* **2015**, *11* (6), 482–486.
- (9) Dai, X.; Yang, Z.; Li, A.; Yang, J.; Ouyang, F. Character of defect states in vacancy-doped MoTe₂ monolayer: Spatial localization, flat bands and hybridization gap. *Superlattices Microstruct.* **2019**, *130*, 528–538.
- (10) Wang, Y.; Xiao, J.; Zhu, H.; Li, Y.; Alsaid, Y.; Fong, K. Y.; Zhou, Y.; Wang, S.; Shi, W.; Wang, Y.; Zettl, A.; Reed, E. J.; Zhang, X. Structural phase transition in monolayer MoTe₂ driven by electrostatic doping. *Nature* **2017**, *550* (7677), 487–491.
- (11) Zakhidov, D.; Rehn, D. A.; Reed, E. J.; Salleo, A. Reversible Electrochemical Phase Change in Monolayer to Bulk-like MoTe₂ by Ionic Liquid Gating. *ACS Nano* **2020**, *14* (3), 2894–2903.
- (12) Song, S.; Keum, D. H.; Cho, S.; Perello, D.; Kim, Y.; Lee, Y. H. Room Temperature Semiconductor–Metal Transition of MoTe₂ Thin Films Engineered by Strain. *Nano Lett.* **2016**, *16* (1), 188–193.
- (13) Tan, S. J. R.; Abdelwahab, I.; Ding, Z.; Zhao, X.; Yang, T.; Loke, G. Z. J.; Lin, H.; Verzhbitskiy, I.; Poh, S. M.; Xu, H.; Nai, C. T.; Zhou, W.; Eda, G.; Jia, B.; Loh, K. P. Chemical Stabilization of 1T'-Phase Transition Metal Dichalcogenides with Giant Optical Kerr Nonlinearity. *J. Am. Chem. Soc.* 2017, 139 (6), 2504–2511.
- (14) Eshete, Y. A.; Ling, N.; Kim, S.; Kim, D.; Hwang, G.; Cho, S.; Yang, H. Vertical Heterophase for Electrical, Electrochemical, and Mechanical Manipulations of Layered MoTe₂. *Adv. Funct. Mater.* **2019**, 29 (40), No. 1904504.
- (15) Chen, S.-Y.; Goldstein, T.; Venkataraman, D.; Ramasubramaniam, A.; Yan, J. Activation of New Raman Modes by Inversion Symmetry Breaking in Type II Weyl Semimetal Candidate T'-MoTe₂. Nano Lett. **2016**, 16 (9), 5852–5860.
- (16) Zhang, K.; Bao, C.; Gu, Q.; Ren, X.; Zhang, H.; Deng, K.; Wu, Y.; Li, Y.; Feng, J.; Zhou, S. Raman signatures of inversion symmetry breaking and structural phase transition in type-II Weyl semimetal MoTe₂. *Nat. Commun.* **2016**, *7* (1), No. 13552.
- (17) Cho, S.; Kim, S.; Kim, J. H.; Zhao, J.; Seok, J.; Keum, D. H.; Baik, J.; Choe, D.-H.; Chang, K. J.; Suenaga, K.; Kim, S. W.; Lee, Y. H.; Yang, H. Phase patterning for ohmic homojunction contact in MoTe₂. Science **2015**, 349 (6248), 625–628.
- (18) Shi, J.; Bie, Y.-Q.; Zong, A.; Fang, S.; Chen, W.; Han, J.; Cao, Z.; Zhang, Y.; Taniguchi, T.; Watanabe, K.; Fu, X.; Bulović, V.; Kaxiras, E.; Baldini, E.; Pablo, J.-H.; Nelson, K. A. Intrinsic 1T' phase induced in atomically thin 2H-MoTe₂ by a single terahertz pulse. *Nat. Commun.* **2023**, *14* (1), No. 5905.
- (19) Wan, J.; Bao, W.; Liu, Y.; Dai, J.; Shen, F.; Zhou, L.; Cai, X.; Urban, D.; Li, Y.; Jungjohann, K.; Fuhrer, M. S.; Hu, L. In Situ Investigations of Li-MoS₂ with Planar Batteries. *Adv. Energy Mater.* **2015**, *5* (5), No. 1401742.
- (20) Xiong, F.; Wang, H.; Liu, X.; Sun, J.; Brongersma, M.; Pop, E.; Cui, Y. Li Intercalation in MoS_2 : In Situ Observation of Its Dynamics and Tuning Optical and Electrical Properties. *Nano Lett.* **2015**, *15* (10), 6777–6784.
- (21) Li, X.; Sun, M.; Cheng, S.; Ren, X.; Zang, J.; Xu, T.; Wei, X.; Li, S.; Chen, Q.; Shan, C. Crystallographic-orientation dependent Li ion migration and reactions in layered MoSe₂. 2D Mater. **2019**, 6 (3), No. 035027.
- (22) Yazdani, S.; Pondick, J. V.; Kumar, A.; Yarali, M.; Woods, J. M.; Hynek, D. J.; Qiu, D. Y.; Cha, J. J. Heterointerface Effects on Lithium-Induced Phase Transitions in Intercalated MoS₂. ACS Appl. Mater. Interfaces **2021**, *13* (8), 10603–10611.
- (23) Pondick, J. V.; Yazdani, S.; Kumar, A.; Hynek, D. J.; Hart, J. L.; Wang, M.; Qiu, D. Y.; Cha, J. J. Thickness-dependent phase transition kinetics in lithium-intercalated MoS₂. 2D Mater. **2022**, 9 (2), No. 025009.

- (24) Zhou, X.; Shu, H.; Li, Q.; Liang, P.; Cao, D.; Chen, X. Electroninjection driven phase transition in two-dimensional transition metal dichalcogenides. *J. Mater. Chem. C* **2020**, 8 (13), 4432–4440.
- (25) Selwyn, L. S.; McKinnon, W. R.; von Sacken, U.; Jones, C. A. Lithium electrochemical cells at low voltage: Decomposition of Mo and W dichalcogenides. *Solid State Ionics* **1987**, 22 (4), 337–344.
- (26) Liu, Y.; Wang, J.; Xu, Y.; Zhu, Y.; Bigio, D.; Wang, C. Lithium—tellurium batteries based on tellurium/porous carbon composite. *J. Mater. Chem. A* **2014**, 2 (31), 12201–12207.
- (27) Froehlicher, G.; Lorchat, E.; Fernique, F.; Joshi, C.; Molina-Sánchez, A.; Wirtz, L.; Berciaud, S. Unified Description of the Optical Phonon Modes in N-Layer MoTe₂. *Nano Lett.* **2015**, *15* (10), 6481–6489
- (28) Ma, X.; Guo, P.; Yi, C.; Yu, Q.; Zhang, A.; Ji, J.; Tian, Y.; Jin, F.; Wang, Y.; Liu, K.; Xia, T.; Shi, Y.; Zhang, Q. Raman scattering in the transition-metal dichalcogenides of $1T'\text{-MoTe}_2$, $T_d\text{-MoTe}_2$, and $T_d\text{-WTe}_2$. Phys. Rev. B **2016**, 94 (21), No. 214105.
- (29) Song, Q. J.; Tan, Q. H.; Zhang, X.; Wu, J. B.; Sheng, B. W.; Wan, Y.; Wang, X. Q.; Dai, L.; Tan, P. H. Physical origin of Davydov splitting and resonant Raman spectroscopy of Davydov components in multilayer MoTe₂. *Phys. Rev. B* **2016**, 93 (11), No. 115409.
- (30) Ruppert, C.; Aslan, B.; Heinz, T. F. Optical Properties and Band Gap of Single- and Few- Layer MoTe₂ Crystals. *Nano Lett.* **2014**, *14* (11), 6231–6236.
- (31) Yamamoto, M.; Wang, S. T.; Ni, M.; Lin, Y.-F.; Li, S.-L.; Aikawa, S.; Jian, W.-B.; Ueno, K.; Wakabayashi, K.; Tsukagoshi, K. Strong Enhancement of Raman Scattering from a Bulk-Inactive Vibrational Mode in Few-Layer MoTe₂. ACS Nano 2014, 8 (4), 3895–3903.
- (32) Iqbal, M. W.; Amin, A.; Kamran, M. A.; Ateeq, H.; Elahi, E.; Hussain, G.; Azam, S.; Aftab, S.; Alharbi, T.; Majid, A. Tailoring the electrical properties of MoTe₂ field effect transistor via chemical doping. *Superlattices Microstruct.* **2019**, *135*, No. 106247.
- (33) Sun, X.; Wang, Z.; Li, Z.; Fu, Y. Q. Origin of Structural Transformation in Mono- and Bi- Layered Molybdenum Disulfide. *Sci. Rep.* **2016**, *6*, No. 26666.
- (34) Sun, L.; Yan, X.; Zheng, J.; Yu, H.; Lu, Z.; Gao, S.-P.; Liu, L.; Pan, X.; Wang, D.; Wang, Z.; Wang, P.; Jiao, L. Layer-Dependent Chemically Induced Phase Transition of Two-Dimensional MoS₂. *Nano Lett.* **2018**, *18* (6), 3435–3440.
- (35) Sear, R. P. Nucleation: theory and applications to protein solutions and colloidal suspensions. *J. Phys.: Condens. Matter* **2007**, *19* (3), No. 033101.
- (36) Wang, M.; Kumar, A.; Dong, H.; Woods, J. M.; Pondick, J. V.; Xu, S.; Hynek, D. J.; Guo, P.; Qiu, D. Y.; Cha, J. J. A Gapped Phase in Semimetallic T_d -WTe $_2$ Induced by Lithium Intercalation. *Adv. Mater.* **2022**, *34* (24), No. 2200861.
- (37) Xu, S.; Wang, M.; Bambrick-Santoyo, M.; Evans-Lutterodt, K.; Williams, N. L.; Cha, J. J. Role of Heterointerface in Lithium-Induced Phase Transition in T_d -WTe₂ Nanoflakes. *ACS Appl. Electron. Mater.* **2024**, *6* (2), 785–792.